respectively. Thus on compression, β-Si_3N_4 will directly transform to c-Si_3N_4 and not to the hypothetical w-Si_3N_4 with lower density. This finding agrees with our synthesis of c-Si_3N_4 above 15 GPa.

The structural parameters for the optimized geometry of c-Si_3N_4 are $a = 7.76$ Å and $\delta = 0.0074$. Fitting a Murnaghan equation of state[23] to the calculated E–V data we obtained a bulk modulus of 300 GPa. This is about 20–30% higher than the experimental values reported for α-Si_3N_4 (229 GPa; ref. 13) and β-Si_3N_4 (250 GPa; ref. 24). Our calculations of the bulk moduli of the α- and β-phase gave 227 GPa and 249 GPa, respectively. Furthermore, we calculated the shear modulus c_{44} to be 340 GPa for c-Si_3N_4 and 150 GPa for β-Si_3N_4.

The calculated bulk and shear c_{44} moduli for c-Si_3N_4 are close to those of stishovite, a high-pressure phase of SiO_2 where the silicon atoms are octahedrally coordinated to oxygen. The high coordination leads to a significant increase in density (4.29 g cm^{-3}; ref. 4), bulk modulus (281–313 GPa; ref. 25) and c_{44} modulus (252 GPa; ref. 26) with respect to the low-pressure modifications of SiO_2 (such as quartz). Moreover, it was found recently that the hardness of SiO_2-stishovite exceeds that of any other known oxide (Knoop hardness 33 GPa; ref. 3). Because the compressibility and the c_{44} modulus of c-Si_3N_4 and SiO_2-stishovite are comparable, we expect that the hardness of c-Si_3N_4 will be close to that of stishovite, which is considered to be the third hardest material after diamond and cubic BN (ref. 3). Because of this, and because of its metastability in air at ambient pressure and high temperatures, c-Si_3N_4 can be considered for technological applications. □

Methods

We calculated[27] the total energies within the local-density approximation (LDA) and the generalized gradient approximation (GGA) of the exchange and correlation energy with standard plane-wave ($E_{cutoff} = 70$ Ry) pseudopotential techniques. Special k-points (10 for c-Si_3N_4 and w-Si_3N_4, 15 for β-Si_3N_4) were used to integrate over the Brillouin zone. At a given volume, the atomic positions were relaxed and in addition for β-Si_3N_4 the c/a ratio was optimized. A detailed description of the method, further calculations and discussions, including differences in results between the LDA or GGA, will be presented elsewhere.

Received 19 February; accepted 25 May 1999.

1. Komeya, K. & Matsui, M. in *Materials Science and Technology* (eds Cahn, R. W., Haasen, P. & Kramer, E. J.) 518–565 (Wiley-VCH, Weinheim, 1994).
2. *Gmelin Handbook of Inorganic and Organometallic Chemistry* Si Suppl. B 5c, *Silicon Nitride in Electronics* (Springer, Berlin, 1991).
3. Leger, J. M. *et al*. Discovery of hardest known oxide. *Nature* **383,** 401 (1996).
4. Smyth, J. R. & McCormick, T. C. in *Mineral Physics and Crystallography: a Handbook of Physical Constants* (ed. Ahrens, T. J.) 1–17 (Am. Geophys. Union, Washington DC, 1995).
5. McCauley, J. W. & Corbin, N. D. Phase relations and reaction sintering of transparent cubic aluminum oxynitride spinel (ALON). *J. Am. Ceram. Soc.* **62,** 476–479 (1979).
6. Grins, J., Käll, P.-O. & Svensson, G. Synthesis, structure and magnetic susceptibility of the oxynitride spinel $Mn_2(MnTa_3)N_{6-\delta}O_{2+\delta}$, $0 < \delta < 1$. *J. Solid State Chem.* **117,** 48–54 (1995).
7. Köllisch, K. & Schnick, W. $Ce_{16}S_{15}O_6M_{32}$-An oxonitridosilicate with silicon octahedrally coordinated by nitrogen. *Angew. Chem. Int. Edn* **38,** 357–359 (1999).
8. Liu, A. Y. & Cohen, M. L. Prediction of new low compressibility solids. *Science* **245,** 841–842 (1989).
9. Teter, D. M. & Hemley, R. J. Low-compressibility carbon nitrides. *Science* **271,** 53–55 (1996).
10. *Powder Diffraction File-2 Database* (JCPDS Int. Centre for Diffraction Data, Newtown Square, PA 19073, USA, 1996).
11. Wada, N., Solin, S. A., Wong, J. & Prochazka, S. Raman and IR absorption spectroscopic studies on α, β and amorphous Si_3N_4. *J. Non-Cryst. Solids* **43,** 7–15 (1981).
12. Bradley, R. S., Munro, D. C., Whitfield, M. The reactivity and polymorphism of selected nitrides at high temperatures and high pressures. *J. Inorg. Nucl. Chem.* **28,** 1803–1812 (1966).
13. Kruger, M. B. *et al*. Equation of state of α-Si_3N_4. *Phys. Rev. B* **55,** 3456–3460 (1997).
14. Yoo, C.-S., Akella, J. & Nicol, M. in *Proc. 3rd Int. Conf. on Advanced Materials* (eds Akaishi, M. et al.) 175–179 (NIRIM, Tsukuba, Japan, 1996).
15. Boehler, R., von Bargen, N. & Chopelas, A. Melting, thermal expansion and phase transitions of iron at high pressures. *J. Geophys. Res.* **95,** 21731–21736 (1990).
16. Boehler, R. & Chopelas, A. A new approach to laser heating in high pressure mineral physics. *Geophys. Res. Lett.* **18,** 1147–1150 (1991).
17. Mernagh, T. P. & Liu, L.-G. Pressure dependence of Raman phonons of some group IVA (C, Si, and Ge) elements. *J. Phys. Chem. Solids* **52,** 507–512 (1991).
18. Bundy, F. P. Phase diagrams of silicon and germanium to 200 kbar, 1000 °C. *J. Chem. Phys.* **41,** 3809–3814 (1964).
19. Olijnyk, H. Raman scattering in metallic Si and Ge up to 50 GPa. *Phys. Rev. Lett.* **68,** 2232–2234 (1992).
20. Kobliska, R. J. *et al*. Raman scattering from phonons in polymorphs of Si and Ge. *Phys. Rev. Lett.* **29,** 725–728 (1972).
21. Yin, M. T. & Cohen, M. L. Theory of static structural properties, crystal stability, and phase transformations: Application to Si and Ge. *Phys. Rev. B* **26,** 5668–5687 (1982).
22. Ihm, J. Total energy calculations in solid state physics. *Rep. Prog. Phys.* **51,** 105–142 (1988).
23. Murnaghan, F. D. The compressibility of media under extreme pressures. *Proc. Natl Acad. Sci. USA* **30,** 244–247 (1944).
24. Cartz, L. & Jorgensen, J. D. The high-pressure behaviour of α-quartz, oxynitride, and nitride structures. *J. Appl. Phys.* **52,** 236–244 (1981).
25. Knittle, E. in *Mineral Physics and Crystallography: a Handbook of Physical Constants* (ed. Ahrens, T. J.) 98–142 (Am. Geophys. Union, Washington DC, 1995).
26. Bass, J. D. in *Mineral Physics and Crystallography: a Handbook of Physical Constants* (ed. Ahrens, T. J.) 45–63 (Am. Geophys. Union, Washington DC, 1995).
27. Bockstedte, M., Kley, A., Neugebauer, J. & Scheffler, M. Density-functional theory calculations for poly-atomic systems: electronic structure, static and elastic properties and ab-initio molecular dynamics. *Comput. Phys. Commun.* **107,** 187–222 (1997).

Acknowledgements. We thank O. Tschauner and I.-W. Chen for discussions, and Bayer AG for providing the β-Si_3N_4 powder. This work was supported by the Deutsche Forschungsgemeinschaft, Bonn, Germany, and the Fonds der Chemischen Industrie, Frankfurt, Germany.

Correspondence and requests for materials should be addressed to R.R. (e-mail: dg9b@hrzpub.tu-darmstadt.de).

Extending the methodology of X-ray crystallography to allow imaging of micrometre-sized non-crystalline specimens

Jianwei Miao*, Pambos Charalambous†, Janos Kirz* & David Sayre*‡

* *Department of Physics and Astronomy, State University of New York, Stony Brook, New York 11794-3800, USA*
† *Kings College, Strand, London WC2R 2LS, UK*

The contrast and penetrating power afforded by soft X-rays when they interact with matter makes this form of radiation ideal for studying micrometre-sized objects[1,2]. But although soft X-rays are useful for probing detail too fine for visible light microscopy in specimens too thick for electron microscopy, the highest-resolution applications of X-ray imaging have been traditionally limited to crystalline samples. Here we demonstrate imaging (at ~75 nm resolution) of a non-crystalline sample, consisting of an array of gold dots, by measuring the soft X-ray diffraction pattern from which an image can be reconstructed. The crystallographic phase problem[3]—the usually unavoidable loss of phase information in the diffraction intensity—is overcome by oversampling[4] the diffraction pattern, and the image is obtained using an iterative algorithm[5]. Our X-ray microscopy technique requires no high-resolution X-ray optical elements or detectors. We believe that resolutions of 10–20 nm should be achievable; this would provide an imaging resolution about 100 times lower than that attainable with conventional X-ray crystallography, but our method is applicable to structures roughly 100 times larger. This latter feature may facilitate the imaging of small whole cells or large subcellular structures in cell biology.

When an object is illuminated by a plane wave, the amplitude of the far-field diffraction pattern is the Fourier transform of the object. The microscopist typically uses a lens to perform the inverse transform to create the image. The resolution of a perfect lens is limited by diffraction to $d > 0.61\lambda/\mathrm{NA}$, where λ is the wavelength and NA is the numerical aperture of the lens. For the visible region of the spectrum, there are high-NA lenses which provide imaging near the limit set by the wavelength, and further improvements are possible using confocal and video techniques.

To get to considerably higher resolution, microscopists use shorter wavelengths, such as are obtained from electrons and X-rays. Transmission electron microscopes routinely image specimens up to ~0.5 μm thick, whereas X-ray microscopes are particularly useful for somewhat thicker specimens which may also be wet[1,2,6,7]. The resolution of X-ray microscopes has been limited by the available optical elements ('optics') to about 30–50 nm (refs 8, 9), and for three-dimensional imaging to about 50–100 nm (refs 10–12) or,

‡ Present address: 15 Jefferson Court, Bridgewater, New Jersey 08807-3050, USA.

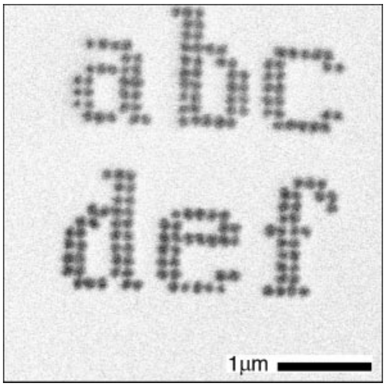

Figure 1 A scanning electron microscope image of the specimen. The specimen was fabricated by depositing gold dots, each ~100 nm in diameter and 80 nm thick, on a silicon nitride membrane.

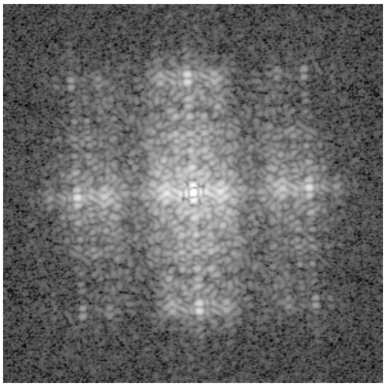

Figure 2 A diffraction pattern of the specimen (using a logarithmic intensity scale). The central 15-pixel-radius circular area is supplied by the squared magnitude of the Fourier transform of the optical microscope image (Fig. 3).

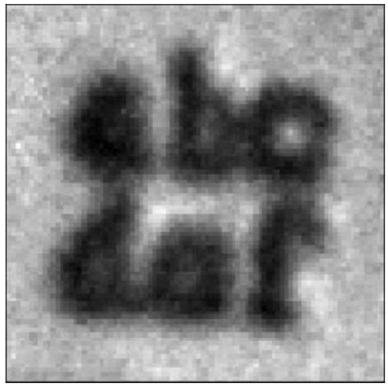

Figure 3 An optical microscope image of the specimen.

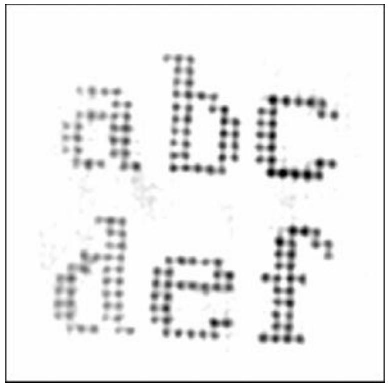

Figure 4 The specimen image as reconstructed from the diffraction pattern of Fig. 2.

in Gabor holography, by the resolution of the detector and/or the optics[13,14].

X-ray crystallography is widely used for very-high-resolution imaging of molecular structure, when these molecules are arranged in a regular crystalline array. This technique requires no optics, and does not impose stringent resolution requirements on the detector. The multiple copies of the specimen amplify the signal, and their regular arrangement concentrates the far-field diffraction pattern into discrete Bragg peaks.

That the general approach of crystallography could be extended to image non-crystalline specimens was first proposed by Sayre in 1980[15]. This approach, although it poses particular challenges in recording and reconstructing the diffraction pattern[16], has the potential to extend the resolution of three-dimensional X-ray microscopy beyond the technical limitations mentioned above, through extending the class of structures to which the powerful techniques of X-ray crystallography can be applied. Here we report the first (to our knowledge) successful recording and reconstruction of such an X-ray diffraction pattern.

The specimen was a collection of gold dots, each ~100 nm in diameter and 80 nm thick, deposited on a 100-nm-thick silicon nitride membrane, to form a set of six letters (Fig. 1). This specimen was illuminated with $\lambda = 1.7$ nm monochromatic and parallel X-rays from the X1A undulator beamline at the National Synchrotron Light Source. To ensure spatial coherence of the illumination, a 10-µm-diameter pinhole was placed at a distance of 2.5 cm upstream of the specimen. To limit the effect of the scatter from the edge of this pinhole, the specimen was placed only ~30 µm from the corners of the silicon nitride membrane, allowing the silicon support to protect three quadrants of the detector from the scatter. In addition, the pinhole served to reduce the size of beam-stop needed to protect the detector from the direct beam; a 220-µm-diameter wire placed in front of the detector was used as beam stop. The detector—a back-thinned, liquid-nitrogen-cooled CCD with 512×512 pixels and a $24\,\mu m \times 24\,\mu m$ pixel size—was placed downstream of the specimen at a distance of 25 cm. A photodiode could be inserted between the beam stop and the CCD to monitor the beam intensity in the presence or absence of pinhole, beam stop and specimen, and to help align these components in the beam. The apparatus was in vacuum with an air-lock for rapid sample change. A typical diffraction pattern is shown in Fig. 2, in which the fourth-quadrant data were obtained by using central symmetry. Since the central region was obscured by the beam stop, we replaced the central area of the X-ray diffraction pattern by a patch from the squared magnitude of the Fourier transform of an optical microscope image of the specimen shown in Fig. 3. The patch is a circular area with a 15-pixel radius, which occupies less than 0.5% of the whole diffraction pattern. The exposure time of the pattern was 15 min which corresponds to an incident flux of 1.65×10^{19} photons m^{-2}, or a radiation dose of 1.56×10^{6} gray (Gy) to the specimen. The pattern extends to the edge of the CCD, suggesting that a larger detector would directly lead to higher spatial resolution.

The intensity of the diffraction pattern provides a record of the size, but not the phase, of the diffraction amplitude. To reconstruct the image, one faces therefore the 'phase problem' of crystallography. The situation for the non-crystalline specimen is different, however, in that the pattern is continuous rather than limited to discrete Bragg peaks. This continuous pattern can therefore be sampled on a finer scale. That sufficient oversampling can lead to a reconstruction was pointed out by Bates[4]. To perform such a reconstruction, Chapman[2] devised a Fienup-type[17] iterative algorithm. Using a strengthened form of this, Miao *et al.*[5] were able not only to perform reconstructions of model data in two and three dimensions, but also to show that the degree of oversampling called for by Bates[4] can be relaxed somewhat for the higher-dimensional cases.

In our experiment we made use of this reconstruction algorithm. The reconstruction from the diffraction pattern of Fig. 2 is shown in Fig. 4. Our phasing algorithm uses knowledge of a finite support which is defined as an enclosing boundary of the specimen. In this reconstruction, we chose a 5.7 μm × 5.7 μm square as the finite support which is larger than the size of the image itself. The initial input to the iterative algorithm was a random phase set and, after about 1,000 iterations, a good reconstruction (Fig. 4) was obtained. The computing time of 1,000 iterations is ~30 min on a 450-MHz Pentium II workstation. Details of the reconstruction procedure are given elsewhere[5,16]. The reconstructed image is consistent with the resolution limit, ~75 nm, set by the angular extent of the CCD detector. The inner portion of the diffraction pattern could also be filled by Fourier processing of a moderate-resolution image of the specimen made with a scanning transmission X-ray microscope[1], whereupon a reconstruction with an almost perfectly clean background was obtained.

We believe that the successful recording and reconstruction of the test pattern reported here is the critical step that will open the way to high-resolution three-dimensional imaging of such structures as small whole cells, or large sub-cellular structures, in cell biology. Extension from two to three dimensions requires that a series of diffraction patterns be recorded as the specimen is rotated around an axis perpendicular to the beam. We have take the first steps in this direction. Model calculations indicate that the iterative algorithm used in this work is able to reconstruct such a data set[5]. To be able to collect the data set from a biological (or other radiation-sensitive) specimen, it would be necessary to keep the specimen near the temperature of liquid nitrogen. Experiments show that specimens at this temperature can withstand a radiation dose up to 10^{10} Gy without observable morphological damage[18,19]. Finally, to improve the resolution without sacrificing specimen size, a CCD detector with more pixels would be needed: such detectors are now commercially available. □

Received 24 March; accepted 8 June 1999.

1. Kirz, J., Jacobsen, C. & Howells, M. Soft X-ray microscopes and their biological applications. *Q. Rev. Biophys.* **28,** 33–130 (1995).
2. Sayre, D. & Chapman, H. N. X-ray microscopy. *Acta Crystallogr. A* **51,** 237–252 (1995).
3. Millane, R. P. Phase retrieval in crystallography and optics. *J. Opt. Soc. Am. A* **7,** 394–411 (1990).
4. Bates, R. H. T. Fourier phase problems are uniquely solvable in more than one dimension. I: underlying theory. *Optik* **61,** 247–262 (1982).
5. Miao, J., Sayre, D. & Chapman, H. N. Phase retrieval from the magnitude of the Fourier transforms of non-periodic objects. *J. Opt. Soc. Am. A* **15,** 1662–1669 (1998).
6. Sayre, D., Kirz, J., Feder, R., Kim, D. M. & Spiller, E. Potential operating region for ultrasoft X-ray microscopy of biological specimens. *Science* **196,** 1339–1340 (1977).
7. Jacobsen, C. & Kirz, J. X-ray microscopy with synchrotron radiation. *Nature Struct. Biol.* **5,** (synchrotron suppl.), 650–653 (1998).
8. Jacobsen, C., Kirz, J. & Williams, S. Resolution in soft X-ray microscopes. *Ultramicroscopy* **47,** 55–79 (1992).
9. Thieme, J., Schmahl, G., Umbach, E. & Rudolph, D. (eds) *X-ray Microscopy and Spectromicroscopy* (Springer, Berlin, 1998).
10. Haddad, W. S. *et al.* Ultra high resolution x-ray tomography. *Science* **266,** 1213–1215 (1994).
11. Lehr, L. 3D x-ray microscopy: tomographic imaging of mineral sheaths of bacteria *Leptothrix ochracea* with the Göttingen x-ray microscope at BESSY. *Optik* **104,** 166–170 (1997).
12. Wang, Y., Jacobsen, C., Maser, J. & Osanna, A. Soft x-ray microscopy with cryo STXM: II. Tomography. *J. Microsc.* (in the press).
13. Howells, M. *et al.* X-ray holograms at improved resolution: a study of zymogen granules. *Science* **238,** 514–517 (1987).
14. Lindaas, S., Howells, M., Jacobsen, C. & Kalinovsky, A. X-ray holographic microscopy by means of photoresist recording and atomic-force microscope readout. *J. Opt. Soc. Am. A* **13,** 1788–1800 (1996).
15. Sayre, D. in *Imaging Processes and Coherence in Physics* (eds Schlenker, M. *et al.*) 229–235 (Springer, Berlin, 1980).
16. Sayre, D., Chapman, H. N. & Miao, J. On the extendibility of X-ray crystallography to noncrystals. *Acta Crystallogr. A* **54,** 233–239 (1998).
17. Fienup, J. R. Phase retrieval algorithm: a comparison. *Appl. Opt.* **21,** 2758–2769 (1982).
18. Schneider, G. & Niemann, B. in *X-ray Microscopy and Spectromicroscopy* (eds Thieme, J., Schmahl, G., Rudolph, D. & Umbach, E.) 25–34 (Springer, Berlin, 1998).
19. Maser, J. *et al.* in *X-ray Microscopy and Spectromicroscopy* (eds Thieme, J., Schmahl, G., Rudolph, D. & Umbach, E.) 35–44 (Springer, Berlin, 1998).
20. Lindaas, S. *et al.* in *X-ray Microscopy and Spectromicroscopy* (eds Thieme, J., Schmahl, G., Rudolph, D. & Umbach, E.) 75–86 (Springer, Berlin, 1998).

Acknowledgements. The decision to try oversampling as a phasing technique was arrived at in a conversation in the late 1980s with G. Bricogne. W. Yun and H. N. Chapman also participated in early parts of this experiment. We thank C. Jacobsen for help and advice, especially with the numerical reconstruction, and we thank him and M. Howells for use of the apparatus[20] in which the exposures were made; we also thank S. Wirick for help with data acquisition. P.C. thanks the Leverhulme Trust Great Britain for supporting the nanofabrication programme at King's College, London. This work was performed at the National Synchrotron Light Source, which is supported by the US Department of Energy. Our work was supported in part by the US Department of Energy.

Correspondence and requests for materials should be addressed to J.M. (e-mail: miao@xray1.physics.sunysb.edu).

Forcing of the cold event of 8,200 years ago by catastrophic drainage of Laurentide lakes

D. C. Barber*, A. Dyke†, C. Hillaire-Marcel‡, A. E. Jennings*, J. T. Andrews*, M. W. Kerwin*, G. Bilodeau‡, R. McNeely†, J. Southon§, M. D. Morehead* & J.-M. Gagnon‖

* *Institute for Arctic & Alpine Research, and Department of Geological Sciences, University of Colorado, Boulder, Colorado 80309, USA*
† *Geological Survey of Canada, 601 Booth Street, Ottawa K1A 0E8, Canada*
‡ *Centre de recherche en géochimie isotopique et en géochronologie, Université du Québec à Montreal, Québec H3C 3P8, Canada*
§ *Center for Accelerator Mass Spectrometry, L-397, Lawrence Livermore National Laboratory, PO Box 808, Livermore, California 94551, USA*
‖ *Canadian Museum of Nature, PO Box 3443, Station D, Ottawa, Ontario K1P 6P4, Canada*

The sensitivity of oceanic thermohaline circulation to freshwater perturbations is a critical issue for understanding abrupt climate change[1]. Abrupt climate fluctuations that occurred during both Holocene and Late Pleistocene times have been linked to changes in ocean circulation[2–6], but their causes remain uncertain. One of the largest such events in the Holocene occurred between 8,400 and 8,000 calendar years ago[2,7,8] (7,650–7,200 ^{14}C years ago), when the temperature dropped by 4–8 °C in central Greenland[2] and 1.5–3 °C at marine[4,7] and terrestrial[7,8] sites around the north-eastern North Atlantic Ocean. The pattern of cooling implies that heat transfer from the ocean to the atmosphere was reduced in the North Atlantic. Here we argue that this cooling event was forced by a massive outflow of fresh water from the Hudson Strait. This conclusion is based on our estimates of the marine ^{14}C reservoir for Hudson Bay which, in combination with other regional data, indicate that the glacial lakes Agassiz and Ojibway[9–11] (originally dammed by a remnant of the Laurentide ice sheet) drained catastrophically ~8,470 calendar years ago; this would have released >10^{14} m^3 of fresh water into the Labrador Sea. This finding supports the hypothesis[2,7,8] that a sudden increase in freshwater flux from the waning Laurentide ice sheet reduced sea surface salinity and altered ocean circulation, thereby initiating the most abrupt and widespread cold event to have occurred in the past 10,000 years.

During the period of deglaciation that preceded the abrupt climate event of 8,400–8,000 calendar years (cal. yr) ago (the '8.2-kyr event'), a remnant Laurentide ice mass occupied Hudson Bay and served as an ice dam for glacial lakes Agassiz and Ojibway[9–12] (Fig. 1). The rapid collapse of ice in Hudson Bay allowed lakes Agassiz and Ojibway, which had previously discharged over spillways southeastwards to the St Lawrence estuary, to drain swiftly northwards through the Hudson Strait to the Labrador Sea[10,13–15].